2D MoS₂ Based Threshold Switching Memristor For Artificial Neuron

Durjoy Dev, *Student Member, IEEE*, Adithi Krishnaprasad, Mashiyat S. Shawkat, Zhezhi He, *Student Member, IEEE*, Sonali Das, Deliang Fan, *Member, IEEE*, Hee-Suk Chung, Yeonwoong Jung, and Tania Roy, *Member, IEEE*

Abstract— In this work, we use a two-terminal 2D MoS₂-based memristive device to emulate an artificial neuron. The Au/MoS₂/Ag device exhibits volatile resistance switching characteristics with a low threshold voltage and a high ON-OFF ratio of 10⁶, originating from an Ag diffusion-based filamentary process. The leaky integrate-and-fire neuron implemented with this device successfully emulates the key characteristics of a biological neuron.

Index Terms - 2D Material, LIF Neuron, MoS2, SNN, TSM

I. INTRODUCTION

PIKING neural network (SNN) mimics the human brain Omost faithfully among all neural networks and are projected to be the most energy-efficient in processing temporal data. The artificial neuron and synapse are the building blocks of SNN. Initially the hardware for SNNs was implemented with complex complementary metal oxide semiconductor (CMOS) circuitry where a single neuron or synapse was realized with multiple transistors, which is intensive in terms of area and energy consumption [1]. The discovery of the memristor in 2008 proliferated the realization of artificial synapses using a single two-terminal device [2], [3]. However, despite the equal importance of artificial neurons, the use of a single device to realize artificial neurons is not wellexplored. Recently, threshold switching memristor (TSM) devices [4], non-volatile memristors [5], phase change materials (PCM) [6], ferroelectric materials-based field effect transistors (FET) [7], [8] and floating body transistors [9] have been utilized to demonstrate leaky integrate-and-fire (LIF) neuron for SNNs. Memristive properties in 2D materials provides opportunities for realizing artificial neurons with these atomically thin systems, which will allow the ultimate vertical scaling of neural network hardware [10]-[12]. H Kalita et al. demonstrated a MoS₂/graphene TSM based artificial neuron but the high threshold voltage, low ON-OFF ratio and low ON

This work is supported by the NSF CAREER Award under grant NSF-ECCS-1845331 and BAE Systems through Award no. 1020180. (Corresponding author: Tania Roy)

Durjoy Dev, Adithi Krishnaprasad, Mashiyat S. Shawkat, Sonali Das, Yeonwoong Jung, and Tania Roy are with NanoScience Technology Center, and Department of Electrical and Computer Engineering, University of Central Florida, Orlando FL 32826, USA.

Yeonwoong Jung, and Tania Roy are with Department of Materials Science and Engineering, University of Central Florida, Orlando FL 32826, USA.

Zhezhi He and Deliang Fan are with School of Electrical, Computer and Energy Engineering, Arizona State University, Tempe, AZ 8528.

Hee-Suk Chung is with Analytical Research Division, Korea Basic Science Institute, Jeonju, Jeollabuk-do 54907, South Korea.

current of the TSM constrained the detail study of LIF neuron and limits its practical utility [11]. A vertical 2D-memristive structure with stable volatile switching characteristics, operating at a low voltage and providing low ON state resistance required for practical neuromorphic applications has not been developed yet.

In this work, we demonstrate an artificial neuron using chemical vapor deposited (CVD) 2D MoS₂-based TSM. The volatile switching characteristics of the TSM are enabled by a top silver (Ag) electrode. The Au/MoS₂/Ag TSM exhibits volatile switching characteristics with a low threshold voltage and high ON-OFF ratio. Area- and temperature-dependent measurements establish that the volatile switching originates from complex Ag ion dynamics. The TSM device is integrated with a simple RC circuit to emulate a LIF neuron, which exhibits all-or-nothing spiking, threshold-driven firing and stimulus strength-based frequency response like biological neurons and shows controllable variation of temporal response with varying input and circuit parameters.

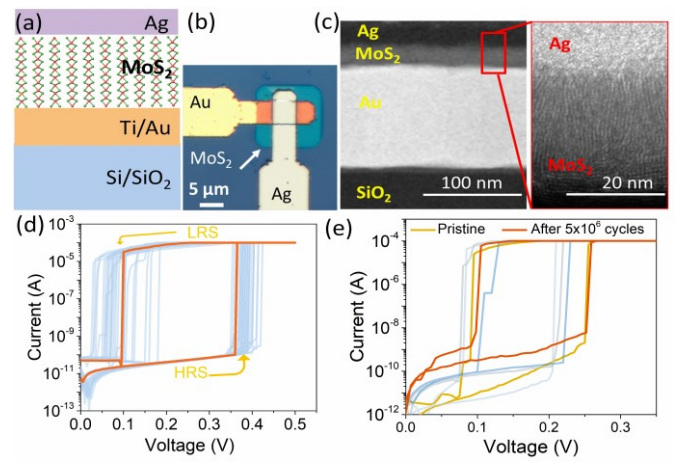


Fig. 1. (a) Schematic and (b) optical image of Au/MoS₂/Ag TSM device. (c) STEM and HRTEM image of cross-section of the vertical stack of MoS₂TSM device. (d) *I-V* characteristics of Au/MoS₂/Ag vertical TSM device with 30 consecutive cycles shown in faded color. (e) *I-V* characteristics of the TSM device at pristine condition and after pulsing for 5×10⁶ cycles with *I-V* for intermediate cycles shown in faded colors (device area 100 μm²).

II. METHODS

The schematic and optical image of the vertical structure Au/MoS₂/Ag TSM is shown in **Fig. 1a-b**. Ti/Au (5/100 nm) bottom electrodes are patterned and deposited on a Si/SiO₂ substrate using standard photolithography and lift-off processes. Mo (10 nm) is patterned and deposited by electron beam evaporation on the bottom electrode. Mo is sulfurized in a low-pressure CVD system at 780 °C to obtain 2D vertically

aligned MoS₂ (~23 nm). The availability of a higher number of dangling bonds and d-orbital electrons at layer edges make vertically-aligned MoS₂ more electrochemically active than horizontally-aligned MoS₂ layers [13]. The top electrode is patterned and Ag/Au (15/40 nm) is deposited by e-beam evaporation on top of MoS₂. The dark-field scanning TEM (STEM) and bright-field high-resolution TEM (HRTEM) characterizations shown in **Fig. 1c** confirms that MoS₂ layers are grown vertically. We perform electrical measurements to characterize the LIF neuron using a B1500A Semiconductor Device Parameter Analyzer on a Micromanipulator probe station (room temperature, in air) and Janis cryogenic probestation (vacuum of 10⁻⁴ Torr, variable temperature).

III. RESULTS AND DISCUSSION

With the application of a positive bias on the top electrode of the TSM device, the device switches sharply from a high resistance state (HRS) to a low resistance state (LRS) at a threshold voltage (V_{th}) of ~0.35-0.4 V, with a high ON-OFF ratio of 10^6 , as shown in **Fig. 1d**. Since the device returns to its HRS during the reverse voltage sweep, it behaves as a threshold switch. The volatile switching in these devices could be attributed to the high thickness of MoS_2 layers, with non-volatility in switching in MoS_2 being observed for thinner films [10], [14]. To investigate the reliability of the switching, continuous pulses of 1.2 V (pulse width 50 μ s and 50% duty cycle) are applied to the device. The device switches to the LRS with every pulse and reverts to the HRS during the OFF time. The *I-V* characteristics of the device in pristine condition and after the application of the 5×10^6 pulsed cycles are shown in **Fig. 1e**.

With the application of appropriate electric field, Ag diffuses from the top electrode through the active channel material and forms a conductive path between the top and bottom electrodes.

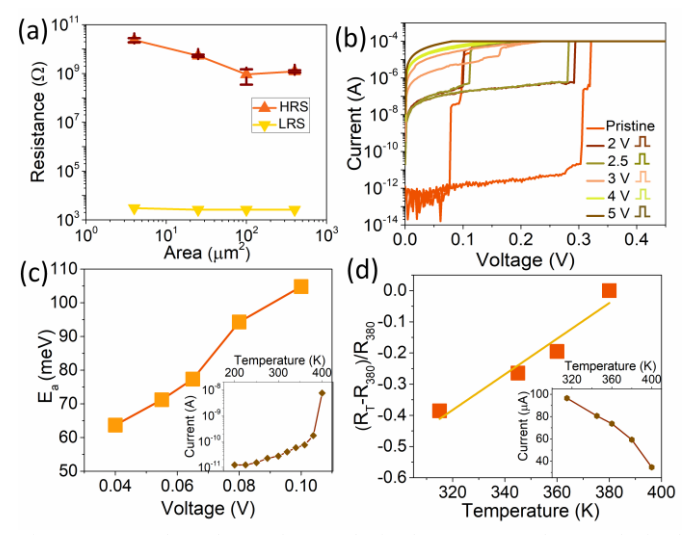


Fig. 2. (a) Area dependence of LRS (obtained at 0.42 V) and HRS (obtained at 0.16 V) of Au/MoS₂/Ag TSM device. (b) *I-V* characteristics of the device in pristine condition and after subjecting the device to voltage pulses of varying amplitudes. (c) The activation energy at different voltages extracted from OFF-state of temperature dependent *I-V* curves. Inset shows increasing trend of OFF-state current with increasing temperature. (d) $(R_T - R_{380})/R_{380}$ vs. T of fully formed TSM device. At fully formed condition, current decreases with increasing temperature (inset). (Device area 4 μ m²)

Upon removal of the electric field, the Ag filament spontaneously turns into a sphere for minimizing the interfacial energy [15]. This behavior facilitates the relaxation of the device by rupturing the conductive filament and enables the volatile behavior. We attribute the threshold switching nature of the Au/MoS₂/Ag device to the formation of Ag conductive filaments through 2D MoS₂ and the self-rupturing of those filaments.

Figure 2a shows the resistance of the TSM device as a function of device area. The almost invariant resistance at LRS with respect to area supports the theory of conduction through localized filaments [16]. The inverse relation between area and HRS is ascribed to the uniform conduction, such as variable range hopping, through polycrystalline MoS₂ [17]. The presence of localized grain boundaries, which limit conduction by scattering, causes the invariant HRS at larger area [16]. The filamentary switching process of the TSM is further confirmed by subjecting the device to voltage pulses with increasing amplitude. Fig. 2b shows the I-V characteristics of the device in pristine condition and after the application of voltage pulses with amplitude 2-5 V and a toN of 1 ms. The increase of the OFF-state current after applying the voltage pulses indicates the formation of a partial conductive path between the top and bottom electrodes [18]. As the voltage pulse amplitude is increased, the conductive filament becomes stronger and the relaxation time increases [15]. Therefore, after applying the pulse of 5 V amplitude, the device remains at LRS, resulting in a "fully formed" condition. These characteristics also support the Ag diffusion-based switching process [19],[20].

Temperature dependent *I-V* measurements are performed on a pristine device and a fully electroformed device to study the conduction mechanism of the Au/MoS₂/Ag structure at HRS and LRS. With increasing temperature, HRS current increases for the pristine device (inset of Fig. 2c), which is similar to the temperature-dependent conductivity of intrinsic semiconducting MoS₂ [17]. The activation energy of the process is extracted from temperature dependent I-V characteristics of the pristine device, using the Arrhenius equation $\sigma(T) = \sigma_0 \exp(-E_a/kT)$ where σ_0 is the conductivity at T = 0 K and k is the Boltzmann's constant. The slope $(-E_a/1000k)$ of the ln σ versus 1000/T plot provides the activation energy. The low activation energy of 62 to 104 meV shown in Fig. 2c, implies variable range hopping conduction in polycrystalline MoS₂ [21]. Fig. 2d (inset) shows that when the device is fully formed, the OFF state current decreases with increasing temperature similar to the electrical characteristics of a metallic conductor, clearly indicating the formation of a metallic path between the two electrodes. This electrochemical formation of the conductive filament can be explained by the excellent ionic mobility of Ag within MoS2 facilitated by the electrochemically active vertically-aligned MoS₂ layers [22]. Temperature coefficient of resistance (TCR) obtained from (R_T) $-R_{380}$)/ R_{380} vs. T plot shown in **Fig. 2d** is 5×10^{-3} K⁻¹, which is the closest match to the TCR of Ag nanowire (3.32×10⁻³ K⁻¹) [23]. Here R_T denotes the resistance at temperature T.

Next, we demonstrate an artificial neuron with the Au/MoS₂/Ag TSM device. The process of generating action potential by biological neuron is explained by a bio-plausible model called "leaky integration and firing" [24]. Electrical

implementation of the LIF model requires a component to integrate the incoming signal and a threshold driven switch to generate the output signal once the threshold is met. The Au/MoS₂/Ag TSM device can emulate the LIF model when integrated with an RC circuit (externally connected on a breadboard, with the TSM device probed in the probe station) as shown in **Fig. 3a**. The RC circuit mimics the integration process of the membrane potential while the ion movement of a biological neuron is emulated by the Ag ion dynamics of a TSM device. **Fig. 3b** shows the multiple current spikes generated from the LIF neuron for a continuous stream of input voltage pulses with 100 μs pulse width and 1 V amplitude.

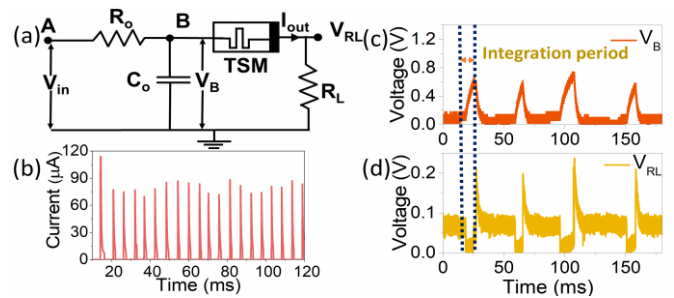


Fig. 3. (a) Circuit diagram for realization of artificial neuron with Au/MoS₂/Ag TSM. (b) Continuous output current spikes from neuron. c) Voltage at node B (V_B). (d) Voltage across load resistor R_L (V_{RL}). (Device area 400 μ m²)

The process of generating output spikes by LIF neuron is elucidated in Fig. 3c-d. Initially the TSM device remains at the HRS and allows a negligible leakage current to flow through load resistor R_L. Therefore, in response to continuous pulses, the capacitor accumulates charge and the potential at node B (V_B) increases, as shown in Fig. 3c. As soon as, V_B reaches the threshold value, the TSM switches to LRS and the capacitor discharges through the load resistor, resulting in an output spike, as shown in Fig. 3d, and the whole process emulates the threshold driven firing behavior of a biological neuron. No response below the threshold voltage and output generated upon surpassing the threshold voltage demonstrate the all-ornothing spiking of a biological neuron. The discharging of the capacitor causes V_B to decrease below V_{th} and the TSM reverts to its HRS. The all-or-nothing spiking behavior of the TSM device enables it to generate output results after producing the first spike in a SNN. For other architectures of artificial neural network (ANN), results are obtained only after processing all the layers. This enables SNN to reduce latency and computational complexity [25].

A certain degree of stochastic behavior is advantageous for enhanced capability and stability of many neuromorphic systems [6], [26]. We perform a statistical analysis of the

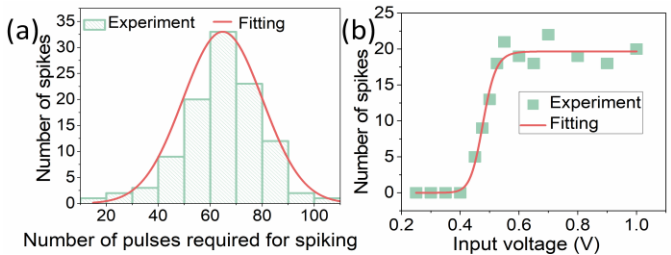


Fig. 4. (a) The normal distribution of variation in the number of pulses required for generating an output spike. (b) The variation of number of output spikes for a given time period with increasing input pulse amplitude. The variation follows sigmoid function. (Device area $400~\mu m^2$)

distribution of output current spikes over a time period of 4 s, consisting of 106 output spikes for 20,000 input voltage pulses. Fig. 4a shows that the number of input voltage pulses required to generate an output spike follows a normal distribution due to the stochastic nature of the device. In a neural network, the activation function determines whether the neuron would be activated or not depending on the weighted synaptic input. Fig. 4b demonstrates the increase in the number of output spikes as the input voltage pulse amplitude is increased, following the sigmoid function most commonly used in SNNs as an activation function.

Figure 5a shows that increasing pulse width facilitates faster charging of input capacitor C_o, hence an increasing number of spikes is observed with increasing pulse width. Increased firing with increasing pulse amplitude and pulse width emulates the stimulus strength-based frequency response of a biological neuron. Conversely, increasing the pulse interval results in decreasing number of output spikes, as shown in Fig. 5b. Reduction of the value of the input capacitance C_o brings down the integration period, resulting in an increased spiking frequency, shown in Fig. 5c. Fig. 5d demonstrates that changing the input resistance while keeping the RC time constant fixed does not affect the output spiking frequency. The ability of tailoring these input pulse and circuit parameters for controlling the firing rates makes the Au/MoS₂/Ag artificial neuron viable for use in neuromorphic applications.

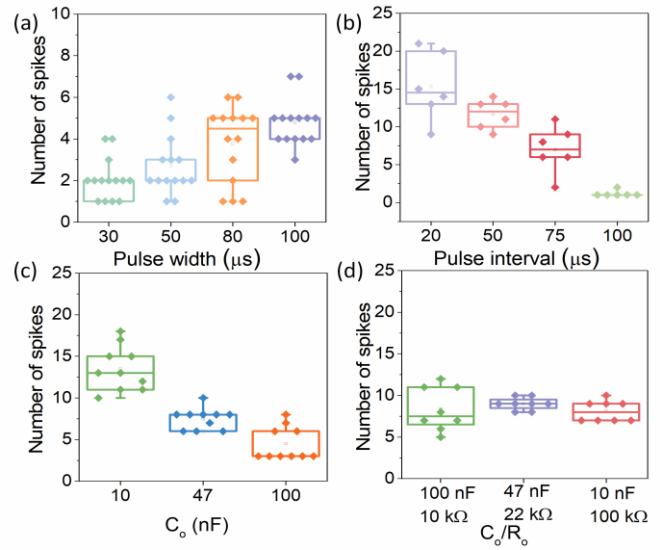


Fig. 5. (a) Increasing pulse width with constant pulse interval and pulse amplitude leads to increasing spiking frequency. (b) Increasing pulse interval with constant pulse amplitude and width results in decreasing spiking frequency. (c) Lower capacitance (C_o) increases the spiking frequency. (d) Variation of both R_o and C_o by keeping RC time constant unchanged does not affect the spiking frequency. (Device area 400 μ m²)

IV. CONCLUSION

In conclusion, Au/MoS₂/Ag memristor devices are fabricated with large area CVD-grown MoS₂. The threshold switching originates from conductive filament formation by Ag diffusion through 2D MoS₂. A LIF neuron with controllable spiking characteristics is realized using the TSM device. The demonstration of artificial neurons with 2D MoS₂ exhibits the viability of this device for future neuromorphic applications and edge computing on a complete 2D platform.

REFERENCES

- [1] G. Indiveri, E. Chicca, and R. Douglas, "A VLSI array of low-power spiking neurons and bistable synapses with spike-timing dependent plasticity," *IEEE Trans. Neural Netw.*, vol. 17, no. 1, pp. 211-221, 2006, doi:10.1109/TNN.2005.860850.
- [2] D. B. Strukov, G. S. Snider, D. R. Stewart, and R. S. Williams, "The missing memristor found," *Nature*, vol. 453, no. 7191, pp. 80, 2008, doi:10.1038/nature06932.
- [3] D. Kuzum, S. Yu, and H. P. Wong, "Synaptic electronics: materials, devices and applications," *J. Nanotechnol.*, vol. 24, no. 38, pp. 382001, 2013, doi:10.1088/0957-4484/24/38/382001.
- [4] D. Lee, M. Kwak, K. Moon, W. Choi, J. Park, J. Yoo, J. Song, S. Lim, C. Sung, W. Banerjee, and H. Hwang, "Various Threshold Switching Devices for Integrate and Fire Neuron Applications," Adv. Electron. Mater., pp. 1800866, 2019, doi:10.1002/aelm.201800866.
- [5] S. Lashkare, S. Chouhan, T. Chavan, A. Bhat, P. Kumbhare, and U. Ganguly, "PCMO RRAM for integrate-and-fire neuron in spiking neural networks," *IEEE Electron Device Lett.*, vol. 39, no. 4, pp. 484-487, 2018, doi:10.1109/LED.2018.2805822.
- [6] T. Tuma, A. Pantazi, M. Le Gallo, A. Sebastian, and E. Eleftheriou, "Stochastic phase-change neurons," *Nat. Nanotechnol.*, vol. 11, no. 8, pp. 693, 2016, doi:10.1038/nnano.2016.70.
- [7] Z. Wang, B. Crafton, J. Gomez, R. Xu, A. Luo, Z. Krivokapic, L. Martin, S. Datta, A. Raychowdhury, and A. I. Khan, "Experimental demonstration of ferroelectric spiking neurons for unsupervised clustering." pp. 13.3. 1-13.3. 4.doi:10.1109/IEDM.2018.8614586.
- [8] Z. Wang, S. Khandelwal, and A. I. Khan, "Ferroelectric oscillators and their coupled networks," *IEEE Electron Device Lett.*, vol. 38, no. 11, pp. 1614-1617, 2017, doi:10.1109/LED.2017.2754138.
- [9] S. Dutta, V. Kumar, A. Shukla, N. R. Mohapatra, and U. Ganguly, "Leaky integrate and fire neuron by charge-discharge dynamics in floating-body MOSFET," *Sci. Rep.*, vol. 7, no. 1, pp. 8257, 2017, doi:10.1038/s41598-017-07418-y.
- [10] A. Krishnaprasad, N. Choudhary, S. Das, D. Dev, H. Kalita, H.-S. Chung, O. Aina, Y. Jung, and T. Roy, "Electronic synapses with near-linear weight update using MoS2/graphene memristors," *Appl. Phys. Lett.*, vol. 115, no. 10, pp. 103104, 2019, doi:10.1063/1.5108899.
- [11] H. Kalita, A. Krishnaprasad, N. Choudhary, S. Das, D. Dev, Y. Ding, L. Tetard, H.-S. Chung, Y. Jung, and T. Roy, "Artificial Neuron using Vertical MoS 2/Graphene Threshold Switching Memristors," Sci. Rep., vol. 9, no. 1, pp. 53, 2019, doi:10.1038/s41598-018-35828-z.
- [12] M. Wang, S. Cai, C. Pan, C. Wang, X. Lian, Y. Zhuo, K. Xu, T. Cao, X. Pan, and B. Wang, "Robust memristors based on layered two-dimensional materials," *Nat. Electron.*, vol. 1, no. 2, pp. 130, 2018, doi:10.1038/s41928-018-0021-4.
- [13] Y. Jung, J. Shen, Y. Liu, J. M. Woods, Y. Sun, and J. J. J. N. l. Cha, "Metal seed layer thickness-induced transition from vertical to horizontal growth of MoS2 and WS2," *Nano Lett.*, vol. 14, no. 12, pp. 6842-6849, 2014, doi:10.1021/nl502570f.
- [14] R. Xu, H. Jang, M.-H. Lee, D. Amanov, Y. Cho, H. Kim, S. Park, H.-j. Shin, and D. Ham, "Vertical MoS2 Double-Layer Memristor with Electrochemical Metallization as an Atomic-Scale Synapse with Switching Thresholds Approaching 100 mV," *Nano Lett.*, vol. 19, no. 4, pp. 2411-2417, 2019, doi:10.1021/acs.nanolett.8b05140.
- [15] Z. Wang, S. Joshi, S. E. Savel'ev, H. Jiang, R. Midya, P. Lin, M. Hu, N. Ge, J. P. Strachan, and Z. Li, "Memristors with diffusive dynamics as synaptic emulators for neuromorphic computing," *Nat. Mater.*, vol. 16, no. 1, pp. 101, 2017, doi:10.1038/nmat4756.
- [16] R. Ge, X. Wu, M. Kim, J. Shi, S. Sonde, L. Tao, Y. Zhang, J. C. Lee, and D. Akinwande, "Atomristor: nonvolatile resistance switching in atomic sheets of transition metal dichalcogenides," *Nano Lett.*, vol. 18, no. 1, pp. 434-441, 2017, doi:10.1021/acs.nanolett.7b04342.
- [17] K. Garadkar, A. Patil, P. Hankare, P. Chate, D. Sathe, and S. Delekar, "MoS2: Preparation and their characterization," *J. Alloys Compd.*, vol. 487, no. 1-2, pp. 786-789, 2009, doi:10.1016/j.jallcom.2009.08.069.
- [18] J. H. Yoon, Z. Wang, K. M. Kim, H. Wu, V. Ravichandran, Q. Xia, C. S. Hwang, and J. J. Yang, "An artificial nociceptor based on a diffusive memristor," *Nat. Commun.*, vol. 9, no. 1, pp. 417, 2018, doi:10.1038/s41467-017-02572-3.

- [19] Y. Yang, P. Gao, S. Gaba, T. Chang, X. Pan, and W. Lu, "Observation of conducting filament growth in nanoscale resistive memories," *Nat. Commun.*, vol. 3, pp. 732, 2012, doi:10.1038/ncomms1737.
- [20] Y. Yang, P. Gao, L. Li, X. Pan, S. Tappertzhofen, S. Choi, R. Waser, I. Valov, and W. D. Lu, "Electrochemical dynamics of nanoscale metallic inclusions in dielectrics," *Nat. Commun.*, vol. 5, pp. 4232, 2014. doi:10.1038/ncomms5232.
- [21] J.-K. Kim, K. Cho, T.-Y. Kim, J. Pak, J. Jang, Y. Song, Y. Kim, B. Y. Choi, S. Chung, and W.-K. Hong, "Trap-mediated electronic transport properties of gate-tunable pentacene/MoS2 pn heterojunction diodes," *Sci. Rep.*, vol. 6, pp. 36775, 2016, doi:10.1038/srep36775.
- [22] P. Wu, N. Yin, P. Li, W. Cheng, and M. Huang, "The adsorption and diffusion behavior of noble metal adatoms (Pd, Pt, Cu, Ag and Au) on a MoS 2 monolayer: a first-principles study," *Phys. Chem. Chem. Phys.*, vol. 19, no. 31, pp. 20713-20722, 2017, doi:10.1039/C7CP04021K.
- [23] Z. Cui, F. R. Poblete, and Y. Zhu, "Tailoring the Temperature Coefficient of Resistance of Silver Nanowire Nanocomposites and their Application as Stretchable Temperature Sensors," ACS Appl. Mater. Interfaces, vol. 11, no. 19, pp. 17836-17842, 2019, doi:10.1021/acsami.9b04045.
- [24] Y. Zhang, W. He, Y. Wu, K. Huang, Y. Shen, J. Su, Y. Wang, Z. Zhang, X. Ji, and G. Li, "Highly Compact Artificial Memristive Neuron with Low Energy Consumption," Small, vol. 14, no. 51, pp. 1802188, 2018, doi:10.1002/smll.201802188.
- [25] R. Midya, Z. Wang, S. Asapu, S. Joshi, Y. Li, Y. Zhuo, W. Song, H. Jiang, N. Upadhay, and M. Rao, "Artificial Neural Network (ANN) to Spiking Neural Network (SNN) Converters Based on Diffusive Memristors," Adv. Electron. Mater., pp. 1900060, 2019, doi:10.1002/aelm.201900060.
- [26] G. Palma, M. Suri, D. Querlioz, E. Vianello, and B. De Salvo, "Stochastic neuron design using conductive bridge RAM." pp. 95-100.doi: 10.1109/NanoArch.2013.6623051.